Metatronic transistor amplifier

Uday K. Chettiar and Nader Engheta

Metatronic Transistor Amplifier

Uday K. Chettiar and Nader Engheta[*]

University of Pennsylvania

Department of Electrical and Systems Engineering

Philadelphia, PA 19104 USA

Abstract

Utilizing the notion of metamaterials, in recent years the concept of a circuit and lumped circuit elements have been extended to the optical domains, providing the paradigm of *optical metatronics, i.e. metamaterial-inspired optical nanocircuitry* as a powerful tool for design and study of more complex systems at the nanoscale. In this Letter we present a design for a new metatronic element, namely, a metatronic transistor that functions as an amplifier. As shown by our analytical and numerical study here, this metatronic transistor provides a gain as well as isolation between the input and output ports of such 2-port device. The cascadability and fan-out aspects of this element are also explored.

[*] To whom correspondence should be addressed. E-mail: engheta@ee.upenn.edu

The recent advances in metamaterial technology have provided us with unprecedented control over designing materials to achieve a wide range of properties [1-3]. The concept of lumped elements is very well established in the realms of electronics and microwave circuits. Extending these concepts to optical frequencies was at first challenging for a multitude of reasons. Firstly, to be considered a lumped element the size of the element should be significantly smaller than the operating wavelength and although this is easily achievable at low frequency and microwave frequencies it is far more challenging at optical frequencies, but this has been achieved using the technology of nanofabrication. Secondly, the material property for conductors (such as metals) is significantly different at optical frequencies compared to lower frequencies. This makes it challenging to easily switch between *wave* mode and *circuit* mode, which is fairly trivial at microwave frequencies due to the availability of efficient conductors, but in metatronics [4-15], which is a confluence of the plethora of well-established techniques in electronics transplanted into the much shorter wavelengths such as optical regimes [4-7], this issue has been dealt with using the displacement currents [6-7, 11-12]. Thirdly, some of the well-developed active lumped elements in the radio frequency (rf) and microwave like semiconductor transistors and diodes may not, in principle, be extended *exactly* to optical frequencies due to the frequency limitation imposed on account of the finite effective mass of the charged carriers. Hence, the evident next stage in the evolution of the field of metatronics is to introduce active elements like transistors, diodes, amplifiers and oscillators.

At microwave frequencies the systems consists of two broad categories of components apart from sources, the first one is the conduits that carry the energy in the

form of modes or waves. For the sake of abstraction, these conduits can be generally considered to be two-port (or multiple-port) structures such as waveguides or transmission lines. The second class of components represents the lumped elements, which could be single-port elements like loads and antennas or multiple-port elements like filters, amplifiers, etc. [16]. The conduits are described using their characteristic impedance and propagation constant, which correspond to the intrinsic wave impedance and refractive index in optical systems. The lumped elements on the other hand are described completely using their scattering parameters (which are also related to their impedances). This abstraction allows us to parameterize, i.e., "hide" the technical details behind the relevant parameters, which results in significant simplifications in the design process. With the above background, how can we conceive the concept of metatronic transistor? At this stage it would be instructive to look at what is implied by a transistor. An electronic transistor is a remarkably versatile device that ends up in a wide array of distinct applications including amplifiers, switches, oscillators, logic devices, etc. [17]. The various different applications are achieved by changing the transistor's mode of operation through different bias settings and by proper design of the supporting circuitry. For example, the amplifier action is achieved by operating the transistor in its active mode while the switching action can be accomplished by swinging the transistor between its cutoff and saturation states [17], while an oscillator action is achieved by biasing it to be in an unstable region [16]. The logic device behavior is typically achieved by combining two complementary field effect transistors to give rise to a CMOS device, which could be operated between the cutoff and the linear mode [17]. It should be apparent at this stage that it is very challenging to design a single metatronic device at the

optical frequencies that could achieve this whole range of tasks that is accomplished by the electronic transistor. In the literature the most common version of optical transistor tends to be a device that functions as a switch [18]. Although an optical switch does represent a critical step in achieving optics-based logic circuits it does not fulfill the other roles played by a transistor like amplifiers and oscillators. Also an optical switch needs to satisfy a list of stringent requirements before it could be considered as an optical logic element [19], some of which are also applicable to amplifiers. In the current work, we present an approach to designing an optical metatronic transistor that functions as an amplifier with the possibility of being operated as an oscillator. Furthermore this design shares several of the desirable properties with microwave amplifiers like input/output isolation, cascadability, fan-out, etc.

Following the inspiration from microwave electronics we look at how a microwave amplifier is implemented in practice. Fig. 1a symbolically shows the schematic of a typical microwave amplifier. The gain is provided by the transistor while the matching circuits ensure that the signal incident on the amplifier from either the input or the output side is not reflected back as this could potentially interfere with the operation of the rest of the system. In order to calculate the gain factor and analyze the stability considerations, all that is needed are the scattering parameters of the two-port device that represents the transistor. The scattering parameters in turn depend on the manner in which the transistor is connected to the system, i.e. common-gate, common-source, etc., the biasing point of the transistor and the supporting circuitry. In order to be a useful building block the amplifier needs to possess certain qualities [19] that includes cascadability, fan-out, input/output isolation and absence of critical biasing. Firstly, we

will focus on input/output isolation. What it essentially implies is that we do not want the signal that is incident on the output port to be transmitted to the input port. This is naturally satisfied in case of a microwave amplifier since in this case the input is usually connected to the gate
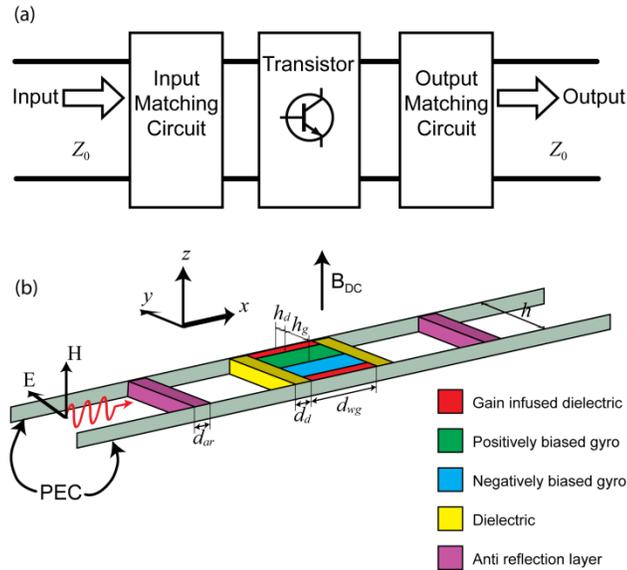
Figure 1. Comparison of microwave and metatronic amplifier. (a) Schematic of a microwave amplifier system. (b) Schematic of a metatronic amplifier system.

of the transistor whereas the output is connected between the source and drain, which provides good isolation between the input and output. In order to implement such a behavior in metatronics we have to necessarily rely on non-reciprocal behavior since the S-matrix for such a two-port device is asymmetric. For this reason we use the one-way gyrotropic waveguide [15] as the component that provides the input/output isolation as shown in Fig. 1b. Furthermore, a microwave amplifier circuit utilizes matching circuits in order to eliminate reflection on both the input and output port. In our metatronic circuit here, this feature could be implemented by using a properly designed anti-reflection layer as shown with purple in Fig. 1b. Finally, in order to realize the desired amplification we

can infuse the dielectric region of the one-way gyrotropic waveguide with gain material [20].

The permittivity of the gyrotropic media (shown as green and blue in Fig. 1b) is given by the following permittivity tensor.

$$\bar{\bar{\varepsilon}} = \varepsilon_0 \begin{pmatrix} \varepsilon_t & i\varepsilon_g & 0 \\ -i\varepsilon_g & \varepsilon_t & 0 \\ 0 & 0 & \varepsilon_n \end{pmatrix}$$

$$\varepsilon_t = 1 - \frac{\omega_p^2(\omega+i\gamma)}{\omega\left((\omega+i\gamma)^2 - \omega_g^2\right)}$$

$$\varepsilon_g = \frac{\omega_p^2\omega_g}{\omega\left((\omega+i\gamma)^2 - \omega_g^2\right)}$$

$$\varepsilon_n = 1 - \frac{\omega_p^2}{\omega(\omega+i\gamma)}$$

Here ω_p is the angular plasma frequency, $\omega_g = eB/m$ is the cyclotron frequency where e is the electron charge, B is the DC biasing magnetic field and m is the effective mass of an electron, and γ is the collision frequency. We have used the $e^{-i\omega t}$ time convention for the complex numbers. The interface between the gyrotropic layer and the dielectric slab (shown as red) supports non-reciprocal surface plasmon polariton (SPP) modes for non-zero values of ω_g [15, 21] (See Appendix A), which acts as a one-way waveguide for a certain frequency range that depends on ω_g. We exploit this feature to achieve the input/output isolation by using a gyrotropic waveguide to construct the transistor as shown in Fig. 1b. The transistor consists of two gyrotropic waveguides which are mirror images of each other (green and blue in Fig. 1b)). Because of the mirror symmetry the ω_g for the two waveguides are opposite in sign in order to ensure the both waveguides support modes propagating in the same direction. In principle it is sufficient to have only

one gyrotropic waveguide (See Appendix A) unless we want an unbounded structure that is periodic in the *y*-direction, unlike the structure that is depicted in Fig. 1b, i.e. bounded in the *y*-direction by perfect electric conductor (PEC). Another set of dielectric layers (shown in yellow in Fig. 1b) bounding the gyrotropic waveguide along the *x*-direction is used to suppress the excitation of unwanted SPPs on the front and back face (*yz* planes) of the gyrotropic media, which could set up a standing wave resulting in increased losses. Furthermore, we also use a pair of anti-reflection (AR) layers in order to eliminate the reflection of incident energy on both sides. These AR layers are designed using the standard quarter-wave transformer method [16] and they are placed at a specific distance from the transistor in order to allow the use of a lossless dielectric as the material for the AR layer. This distance can be obtained by using standard impedance transformation methods [16].

Before we look at the effect of the magnetic bias on the transistor we first consider the propagation of the modes in an unbiased gyrotropic waveguide in the presence of gain. Under the assumption that SPPs are tightly bound [22] and the imaginary part of the permittivity for both the dielectric and plasmonic media is small with respect to the real part we can derive following relation for the real and imaginary parts of the propagation constant [20, 23] (See Appendix A).

$$\frac{\beta'}{k_0} = \sqrt{\frac{\varepsilon'_t \varepsilon'_d}{\varepsilon'_t + \varepsilon'_d}}$$

$$\frac{\beta''}{k_0} = \frac{1}{2}\left(\frac{\varepsilon''_t}{\varepsilon'^2_t} - \frac{\varepsilon''_d}{\varepsilon'^2_d}\right)\left(\frac{\varepsilon'_t \varepsilon'_d}{\varepsilon'_t + \varepsilon'_d}\right)^{3/2}$$

This implies that in order to completely compensate the losses in the plasmonic layer we need to have

$$\varepsilon_d'' = \left(\frac{\varepsilon_d'}{\varepsilon_t'}\right)^2 \varepsilon_t'' \tag{1}$$

The requirement for the gain coefficient is more relaxed for higher values of ε_t'. This makes physical sense since if the permittivity of the plasmonic region is more negative the fields are expelled into the dielectric region and consequently the SPP mode experiences lower loss due to the plasmonic region. The incident signal could also lose power due to reflection. But with a properly designed AR layer we could ensure that none of the signal is reflected back and the only loss mechanism is through the absorption in the plasmonic region. At the interface between the input waveguide and the gyrotropic waveguide the interactions between the two waveguides result in the excitation of several higher-order evanescent modes in addition to the propagating modes. These modes also experience the losses in the plasmonic region and these losses are not accounted by β''. But these additional losses could be numerically evaluated and added to the model as a *coupling loss* (See Appendix A).

Having analyzed the role of the gain medium on the propagation characteristics of the SPP we will now look at the effect of the magnetic bias. It can be shown that for small biases the SPP cut-off frequency for the forward and backward SPPs are separated by ω_g [24].

$$\omega_{spp} = \frac{\omega_p}{\sqrt{1+\varepsilon_d}} \pm \frac{\omega_g}{2}$$

This implies that on application of an appropriate magnetic bias we could operate at a frequency that is ω_g lower than the cutoff frequency for the forward mode while still working in the one-way regime for the gyrotropic waveguide. This has an important

effect on the necessary gain coefficient since a lower frequency of operation implies a more negative plasma permittivity and a consequently relaxed requirement on the gain coefficient in order to compensate the losses due to the plasmonic medium. For small losses and small bias we can assume that under a bias of ω_g we could operate at a frequency that is ω_g below cutoff while still working in the *one-way* regime. Under this condition we can show that for a given bias the required ε_d'' in order to compensate the losses is as follows (See Appendix B).

$$\varepsilon_d'' = \left(1 - 4\frac{\omega_g}{\omega_p}\left(1+\varepsilon_d\right)^{3/2}\right)\varepsilon_m''$$

This is a key relation showing that increasing the magnetic bias could relax the requirement on the gain coefficient. Consequently, if the gain coefficient is limited due to practical consideration we could compensate for it by applying a stronger magnetic bias. But once we achieve a net gain we also have the possibility of tuning it using ε_d'' and ω_g as the control knobs. The effect of changing ε_d'' and ω_g on β' and β'' is discussed in detail in the Appendix B.

We start by presenting the results for a standalone amplifier system as depicted in Fig. 1b, which will be followed by results for cascaded amplifiers and a fan-out system. In order to keep the results as general as possible we will be working in normalized units where the frequency units are normalized with respect to ω_p and the length units are normalized with respect to $\lambda_p = c/\omega_p$. The relative permittivity of the dielectric region in the gyrotropic waveguide is set to $\varepsilon_d = 2.25 - i\varepsilon_d''$. The height of the dielectric and each gyrotropic region is set to $h_d = 0.28\lambda_p$ and $h_g = 0.42\lambda_p$ yielding a total height of $1.4\lambda_p$. The

refractive index of the two SPP-suppressing layers at the front and back of the transistor (shown in yellow in Fig. 1b) is set to 2.5. This ensures that the operating frequency is above the cutoff for the SPPs on the front and back face. The two AR layers have a refractive index (n_{ar}) of 2.52 and a thickness of $0.19\lambda_p$, which corresponds to $\lambda/4n_{ar}$ at the frequency of operation. The AR layers are placed at a distance of $1.05\lambda_p$ from the transistor. The width of the transistor region is set to $4\lambda_p$. The frequency of operation is set to $0.51\omega_p$ for all the results, but this frequency could be easily changed provided the AR layer is redesigned to account for the new frequency of operation. The simulations were performed in a commercial full-wave solver (COMSOL Multiphysics®) using the finite-element method (FEM) in frequency domain with a 2D geometry. Figure 2 shows the results when the bias, ω_g is set to $0.1\omega_p$. At this bias the transistor region shows *one-way* operation for frequencies between $0.5\omega_p$ and $0.6\omega_p$. Since the frequency of operation is set to $0.51\omega_p$ we are operating within the one-way regime. Figure 2a shows two of the four scattering parameters. As is well known, for the reciprocal lossless 2-port network, the scattering matrix is symmetric and unitary. However, here owing to the presence of nonreciprocity and gain in this structure, this matrix is no longer symmetric or unitary. Noting the input and output ports (shown in Fig. 1) as ports "1" and "2", respectively, Fig. 2a reveals that the reflectance ($|S_{11}|^2$) is equal to zero, due to the presence of the AR layer, while the
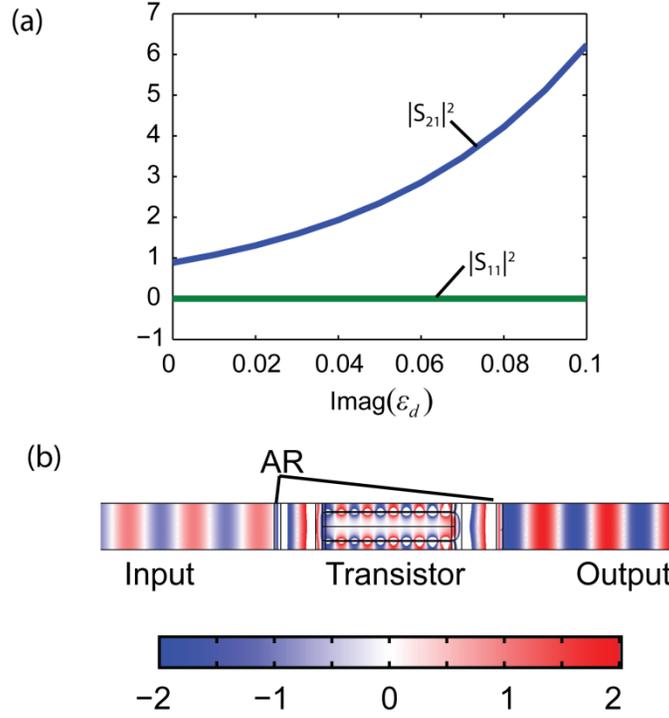
Figure 2. Results for metatronic amplifier when the bias ω_g is set to 0.1 ω_p. (a) parameters. $|S_{22}|^2$ and $|S_{12}|^2$ are indistinguishable from zero and are not shown in the plot. (b) Field map for the magnetic field when imag(ε_d) is set to 0.07.

transmittance ($|S_{21}|^2$) shows an exponential dependence on ε_d''. The scattering parameters for energy incident on the output port (S_{12} and S_{22}) are indistinguishable from zero and not shown in the figure. $|S_{12}|^2$ is zero since we are operating in the one-way regime, while $|S_{22}|^2$ is zero by virtue of the AR layer on the output side of the system. This clearly shows that our metatronic transistor design works as an amplifier and the input is isolated from the output and both input and output ports are impedance matched. As a side note, the zero $|S_{22}|^2$ provides an intriguing possibility of using the structure as a perfect absorber if the signal is incident on the output port.

So far we have looked at the effect of ε_d'' on the scattering parameters. But we can also actively vary the bias (ω_g), which was previously set to $0.1\omega_p$. For the frequency of operation ($0.51\omega_p$) the transistor region shows a one-way response when the bias is set to values above $0.09\omega_p$. Hence we expect the system to show drastically different response for biases above and below $0.09\omega_p$. Figure 3a shows the results for $|S_{21}|^2$ at biases corresponding to the one-way regime. For these biases all other scattering parameters except S_{21} are very close to zero and consequently they are not shown in the figure. We see that for each bias the transmittance increases exponentially with ε_d'', but the rate of increase varies with the bias. Higher bias leads to lower net gain (See Appendix C for the reason). Hence the bias provides an additional mechanism to control the gain of the amplifier. Figs. 3(b-e) show the results for the scattering parameters when the
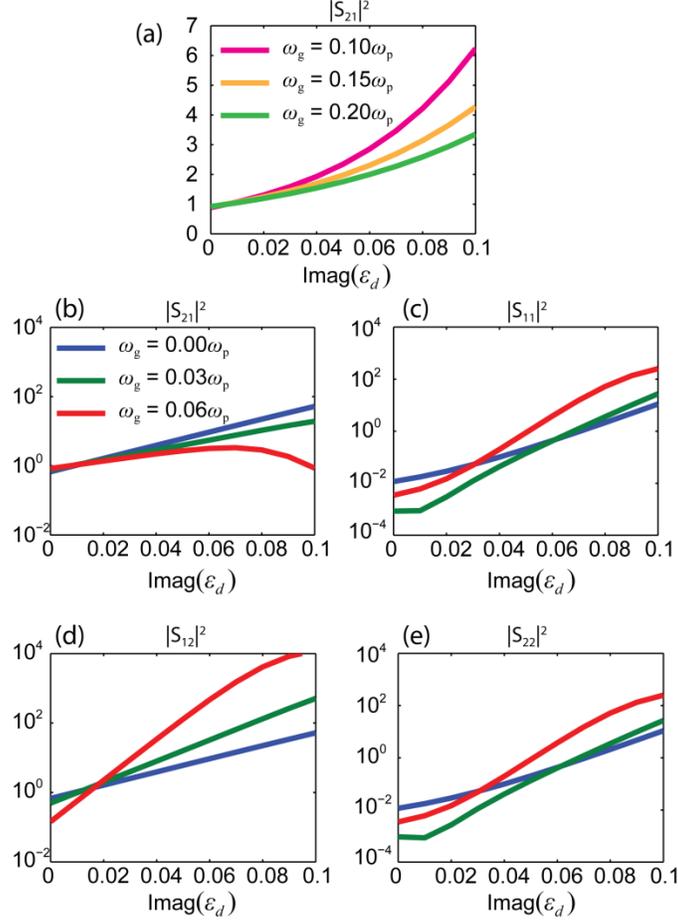
Figure 3. Scattering parameters for the metatronic amplifier under various biases. (a) $|S_{21}|^2$ for the metatronic amplifier when the bias ω_g is set to $0.1\omega_p$, $0.15\omega_p$ and $0.2\omega_p$. All these biases correspond to the one-way regime and for these biases $|S_{21}|^2$, $|S_{22}|^2$ and $|S_{12}|^2$ are indistinguishable from zero. (b)$|S_{21}|^2$, (c)$|S_{11}|^2$, (b)$|S_{12}|^2$ and (b)$|S_{22}|^2$ when the bias ω_g is set to 0, $0.03\omega_p$ and $0.06\omega_p$. These biases correspond to the two-way regime. The operation frequency for all the results was set to $0.51\ \omega_p$.

bias is not sufficiently high to ensure one-way operation. Under this bias we can see significantly higher gain albeit at the cost of giving up the input/output isolation (as seen from $|S_{12}|^2$) and non-zero reflection. Interestingly $|S_{11}|$ and $|S_{22}|$ are exactly identical in spite of the structure being non-reciprocal. This does not violate any laws as the non-reciprocity relates S_{12} and S_{21}.

The primary reason for designing an amplifier with zero reflection is that it will enable us to easily cascade multiple amplifier and get a predictable gain for the cascaded system. The net gain will simply be the product of the gain of all the constituent amplifiers in the cascade. To test this hypothesis we simulated a cascade of two identical metatronic amplifiers as shown in Fig. 4a. The resulting scattering parameters are shown in Fig. 4b. As expected, even for the cascaded system the reflectance ($|S_{11}|^2$) is zero. The net transmittance ($|S_{21}|^2$) is identical to the square of the transmittance for a single amplifier as shown in Fig. 2a. Similarly the input/output isolation coupled with the
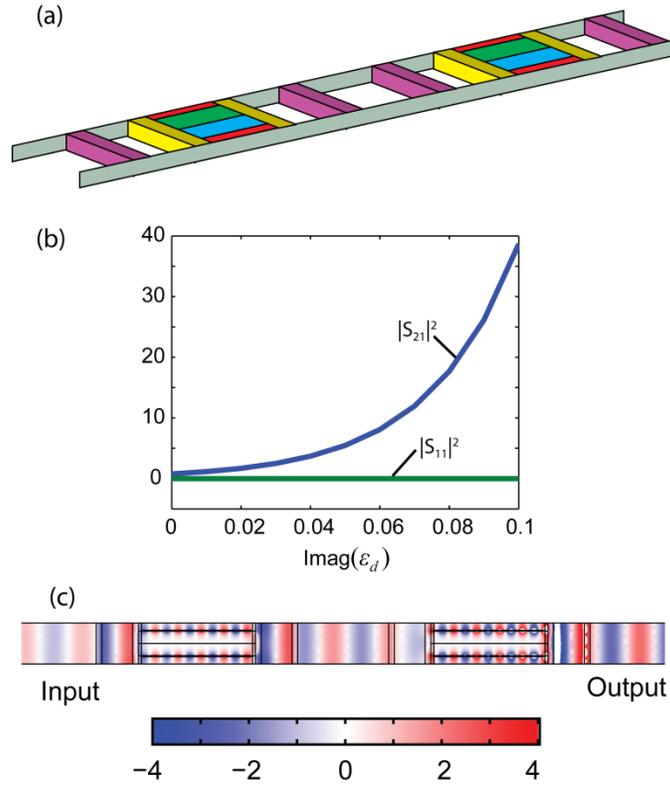
Figure. 4. Schematic and results for a cascaded metatronic amplifier. (a) Schematic. (b) Scattering parameters for cascaded metatronic amplifier when the bias ω_g is set to 0.1 ω_p. $|S_{22}|^2$ and $|S_{12}|^2$ are indistinguishable from zero and are not shown in the plot. (c) Field map for the magnetic field when imag(ε_d) is set to 0.05.
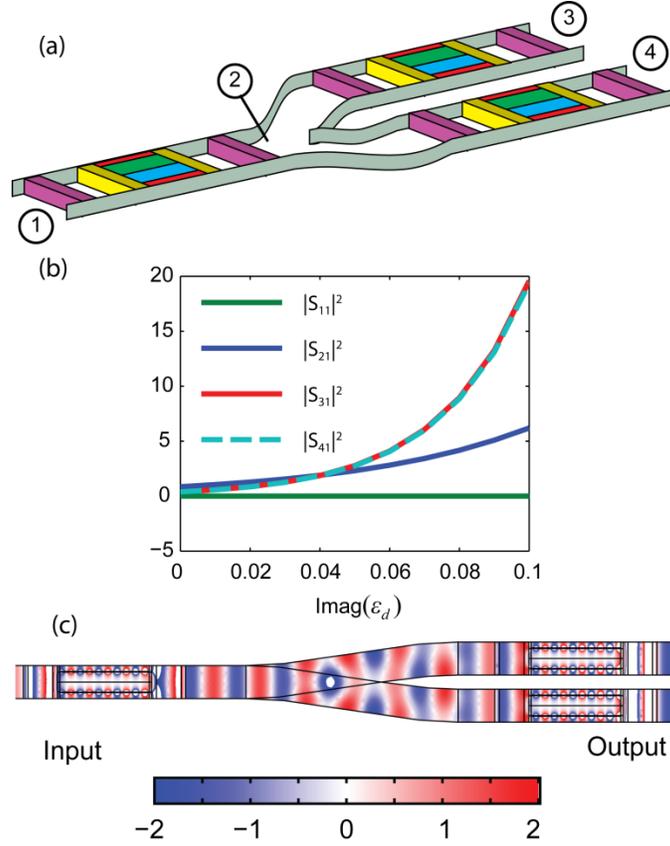
Figure. 5. Schematic and results for a fanned out metatronic amplifier. (a) Schematic. (b) Scattering parameters for cascaded metatronic amplifier when the bias ω_g is set to 0.1 ω_p. Only scattering parameters with input in port 1 are shown in the figure. All other scattering parameters are indistinguishable from zero. (c) Field map for the magnetic field when imag(ε_d) is set to 0.05.

zero reflection allowed us to easily fan-out the output from one amplifier to multiple amplifiers. Fig. 5a shows the schematic of such a case. The simulation results are shown in Fig. 5b and as expected the net gain at ports 3 and 4 are equal to half of the net gain achieved with the cascaded system in Fig. 4b.

At this stage it would be instructive to discuss the possible avenues for the implementation of this transistor. For simplicity we have assumed a PEC wall as the boundary for the system. This would work as a good approximation for noble metals in

the mid IR wavelength and even near IR wavelengths as long as the wavelength of operation is not too close to the visible range. In case the wavelength of operation is closer to the visible wavelengths the PEC boundary could be replaced with a photonic crystal boundary to obtain similar results [21]. Regarding the plasmonic material, at visible wavelengths the noble metals would serve as a good candidate. In case the operating wavelength is desired to be in the near or mid IR one could use other materials in transparent conducting oxides such as indium tin oxide or aluminum-doped zinc oxide [25]. The cyclotron frequency (ω_g) that we have used in the simulations is about 10% of the plasma frequency (ω_p). This is indeed high if we consider the plasma frequency of noble metals. But by working in the near to mid IR or THz regime we could bring down the requirements for the DC magnetic bias. As an alternative one may also consider using magneto-optical material which shows a stronger gyrotropic response [26]. Finally, the gain material could be any material that could be embedded in a dielectric and pumped (either optically or electrically) in order to achieve population inversion. Rhodamine 6G embedded in polymethyl methacrylate (PMMA) has been used to extend the propagation length of SPP [20] and a similar approach could be used to implement the metatronic transistor presented here. As possible paths for future investigation one may also explore the potential role of miniaturization and slow-wave structures for possible enhancement of gain effect [27,28] and the effect of noise and nonlinearity in such metatronic devices.

We have extended the theory of metatronics to include a transistor that functions as an amplifier. This metatronic transistor provides good input/output isolation while enabling a tunable amplifier gain. The transistor could also be easily combined with anti-reflection layers to provide zero reflection on both the input and output ports. The

addition of an amplifier to metatronics will enable the design of more complex systems that could achieve further advances in nanoscale optical signal processing. We also envision the possibility of using the metatronic amplifier to create a metatronic oscillator by using a broadband gain medium and biasing the amplifier in an unstable state. This is currently being explored.

ACKNOWLEDGEMENT

APPENDICES

A.   DISPERSION EQUATION

We begin by analyzing the dispersion equation for the waveguide shown in Fig. 6. The figure essentially depicts one half of the transistor region that is studied in the manuscript. Since the other half of the transistor region is the mirror image of the section shown in Fig. 6 and moreover it is oppositely biased it is adequate to evaluate the dispersion of just one-half of the waveguide in order to analyze the propagation characteristics and scattering parameters of the whole amplifier. The waveguide consists of a layer of gain-infused dielectric and a layer of biased gyrotropic medium. The thickness of the dielectric (gain) layer and the gyrotropic layer is h_d and h_g, respectively. The magnetic bias is applied along the z-direction (Voigt configuration). The magnetic field of the mode is polarized along the z-direction while the electric field lies in the xy plane. The waveguide is bounded in the y-direction by PEC plates.
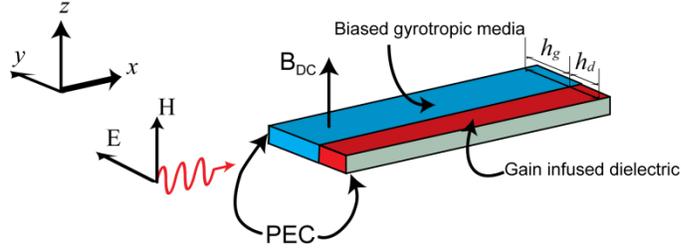
Figure. 6. Schematic of the waveguide analyzed for the dispersion characteristics.

The permittivity of the gyrotropic media is given by the following permittivity tensor.

$$\overline{\overline{\varepsilon}} = \varepsilon_0 \begin{pmatrix} \varepsilon_t & i\varepsilon_g & 0 \\ -i\varepsilon_g & \varepsilon_t & 0 \\ 0 & 0 & \varepsilon_n \end{pmatrix}$$

$$\varepsilon_t = 1 - \frac{\omega_p^2(\omega+i\gamma)}{\omega\left((\omega+i\gamma)^2 - \omega_g^2\right)}$$

$$\varepsilon_g = \frac{\omega_p^2\omega_g}{\omega\left((\omega+i\gamma)^2 - \omega_g^2\right)}$$

$$\varepsilon_n = 1 - \frac{\omega_p^2}{\omega(\omega+i\gamma)}$$

Here ω_p is the angular plasma frequency, $\omega_g = eB/m$ is the cyclotron frequency where e is the electron charge, B is the DC magnetic field and m is the *effective* mass of an electron, and γ is the collision frequency. We have used the $e^{-i\omega t}$ time convention for the complex

numbers. We assume the propagation constant to be β, and the component of the wavevector in the y-direction for the gain is assumed to have the following form.

$$\alpha_d = \sqrt{\beta^2 - k_0^2 \varepsilon_d}$$

Among the two roots the positive root is selected for this term. We also assume the component of the propagation constant along the y-direction for the gyrotropic medium to be α_g although because of the non-diagonal permittivity α_g does not have the same form as α_d and its form will be determined through the application of Maxwell's equations. To derive the dispersion equation we assume the following forms for the magnetic field in the dielectric and the gyrotropic region.

$$\mathbf{H}_d(x,y) = \left(Ae^{\alpha_d y} + Be^{-\alpha_d y} \right) e^{i\beta x} \hat{\mathbf{z}}$$

$$\mathbf{H}_g(x,y) = \left(Ce^{\alpha_g y} + De^{-\alpha_g y} \right) e^{i\beta x} \hat{\mathbf{z}}$$

Using the Maxwell equations we can write the electric field in the following form.

$$\mathbf{E}_d(x,y) = \frac{1}{\varepsilon_d \omega} e^{i\beta x} \left[i\alpha_d \left(Ae^{\alpha_d y} - Be^{-\alpha_d y} \right) \hat{\mathbf{x}} + \beta \left(Ae^{\alpha_d y} + Be^{-\alpha_d y} \right) \hat{\mathbf{y}} \right]$$

$$\mathbf{E}_g(x,y) = \frac{1}{\varepsilon_t \varepsilon_v \omega} e^{i\beta x} \left[\begin{array}{l} i\left\{ Ce^{\alpha_m y} \left(\alpha_m \varepsilon_t + \beta \varepsilon_g \right) - De^{-\alpha_m y} \left(\alpha_m \varepsilon_t - \beta \varepsilon_g \right) \right\} \hat{\mathbf{x}} \\ + \left\{ Ce^{\alpha_m y} \left(\beta \varepsilon_t + \alpha_m \varepsilon_g \right) + De^{-\alpha_m y} \left(\beta \varepsilon_t - \alpha_m \varepsilon_g \right) \right\} \hat{\mathbf{y}} \end{array} \right]$$

Where ε_d is the permittivity of the dielectric and $\varepsilon_V = \varepsilon_t - \varepsilon_g^2 / \varepsilon_t$ is termed as the Voigt permittivity of the gyrotropic medium. Also, the component of the wavevector in the y-direction within the gyrotropic region is given by $\alpha_g = \sqrt{\beta^2 - k_0^2 \varepsilon_V}$. Applying the appropriate boundary conditions yields the following dispersion equation.

$$\frac{\alpha_d \alpha_g \varepsilon_t}{\alpha_g \varepsilon_t + \beta \varepsilon_g} \tanh\left(\alpha_d h_d\right) + \frac{\varepsilon_d \left(\alpha_g \varepsilon_t - \beta \varepsilon_g\right)}{\varepsilon_t \varepsilon_v} \tanh\left(\alpha_g h_g\right)$$
$$+ \frac{\alpha_d \varepsilon_g \beta}{\beta \varepsilon_g + \alpha_g \varepsilon_t} \tanh\left(\alpha_d h_d\right) \tanh\left(\alpha_g h_g\right) = 0 \tag{2}$$

Owing to the transcendental nature of the equation it is not possible to obtain a closed form expression for the propagation constant, but the equation could be readily solved using elementary numerical methods like the simplex method. But in order to gain physical intuition it is instructive to obtain a simplified albeit approximate closed-form expression. At wavelengths where the dielectric-gyrotropic interface supports surface modes (Surface plasmon polaritons, SPPs) the waves in the gyrotropic region is strongly evanescent due to the negative values of the permittivity. Therefore we can safely assume that the plasma region (i.e., the gyrotropic medium) is semi-infinite in the y direction in order to derive an approximate dispersion relation. Under the assumption that $e^{-\alpha_g h_g}$ is close to zero we can show that the dispersion equation reduces to the following.

$$\frac{-\alpha_d \varepsilon_V}{\varepsilon_d} \tanh\left(\alpha_d h_d\right) - \alpha_g + \beta \varepsilon_g / \varepsilon_t = 0 \tag{3}$$

The linear term in β is responsible for the nonreciprocal behavior as it implies that the roots of the dispersion equation no longer come in pairs that are the negatives of each other. Although this dispersion equation is much simpler than the original equation it still does not afford closed-form solutions. For tightly bounded SPPs we can further assume that $e^{-h_d \alpha_d}$ is close to zero. Under this assumption the dispersion relation reduces to $-\alpha_g + \beta \varepsilon_g / \varepsilon_t = \alpha_d \varepsilon_v / \varepsilon_d$. Under zero bias, i.e. $\varepsilon_g = 0$, we arrive at the familiar surface plasmon dispersion relation for a planar interface, $\dfrac{\beta}{k_0} = \sqrt{\dfrac{\varepsilon_t \varepsilon_d}{\varepsilon_t + \varepsilon_d}}$. The plasmonic material

possesses a loss ($\varepsilon_t = \varepsilon'_t + i\varepsilon''_t$) and the dielectric material provides gain ($\varepsilon_d = \varepsilon'_d - i\varepsilon''_d$). Both ε''_d and ε''_t are assumed to be positive. Under the assumption that the imaginary part of the permittivity for both the dielectric and plasmonic media is small with respect to the real part we can derive following relation for the real and imaginary parts of the propagation constant.

$$\frac{\beta'}{k_0} = \sqrt{\frac{\varepsilon'_t \varepsilon'_d}{\varepsilon'_t + \varepsilon'_d}}$$

$$\frac{\beta''}{k_0} = \frac{1}{2}\left(\frac{\varepsilon''_t}{\varepsilon'^2_t} - \frac{\varepsilon''_d}{\varepsilon'^2_d} \right)\left(\frac{\varepsilon'_t \varepsilon'_d}{\varepsilon'_t + \varepsilon'_d} \right)^{3/2}$$

This implies that in order to completely compensate the losses in the plasmonic layer we need to have $\varepsilon''_d = \left(\dfrac{\varepsilon'_d}{\varepsilon'_t} \right)^2 \varepsilon''_t$.

B.   EFFECT OF MAGNETIC BIAS

Having analyzed the role of the gain medium on the propagation characteristics of the SPP we will now look at the effect of the magnetic bias. It can be shown that for small biases the SPP cutoff frequency for the forward and backward SPPs are separated by ω_g. The forward and backward SPP cutoff frequency is given by the following.

$$\omega_{spp} = \frac{\omega_p}{\sqrt{1 + \varepsilon_d}} \pm \frac{\omega_g}{2}$$

This implies that on application of an appropriate magnetic bias we could operate at a frequency that is ω_g lower than the cutoff frequency for the forward mode while still working in the one-way regime for the gyrotropic waveguide. This has an important

effect on the necessary gain coefficient since a lower frequency of operation implies a more negative plasma permittivity and a consequently relaxed requirement on the gain coefficient in order to compensate the losses due to the plasmonic medium. Under zero bias the cutoff is given by $\omega_p/\sqrt{1+\varepsilon_d}$. For small losses and small bias we can assume that under a bias of ω_g we could operate at a frequency that is about ω_g below cutoff while still working in the one-way regime. The real part of the plasmonic material at this operating frequency is given by the following expression to the first order.

$$\frac{\varepsilon_t'}{\varepsilon_d'} = -\left(1 + 2\frac{\omega_g}{\omega_p}\left(1+\varepsilon_d\right)^{3/2}\right)$$

Putting it in the equation for ε_d'' we get the following relation giving the required gain for a certain bias.

$$\varepsilon_d'' = \left(1 - 4\frac{\omega_g}{\omega_p}\left(1+\varepsilon_d\right)^{3/2}\right)\varepsilon_m''$$

By using the equations for the propagation constant and substituting the plasmonic permittivity obtained using the effective plasma frequency we can arrive at the following approximate results for the propagation constant.

$$\frac{\beta'}{k_0} = \sqrt{1 + \frac{\varepsilon_d'}{\dfrac{\omega_p^2 + \omega_p\omega_g\sqrt{1+\varepsilon_d'}}{\omega^2} - 1 - \varepsilon_d'}}\sqrt{\varepsilon_d'}$$

$$\frac{\beta''}{k_0} = \frac{1}{2}\left(\frac{\gamma\omega}{\omega_p^2 + \omega_p\omega_g\sqrt{1+\varepsilon_d'}} - \frac{\varepsilon_d''}{\varepsilon_d'^2}\right)\left(\frac{\beta'}{k_0}\right)^3$$

(4)

For a fixed ε_d'' if we increase ω_g the effect of γ in the expression for β'' reduces indicating that it would be easier to compensate for the loss of the plasmonic material. But once β'' becomes negative we are more concerned about the magnitude of β'' and

this also depend on the third power of β'. To look at the effect of increasing ε_d'' and ω_g

we look at the results for the parameters used in the main manuscript. As in the

manuscript we normalize all the frequency units with ω_p, length units with λ_p and wave

vectors with k_p. The permittivity of the dielectric region in the gyrotropic waveguide is

set to $\varepsilon_d = 2.25 - i\varepsilon_d''$ and the frequency of operation is set to $0.51\omega_p$. The height of the

dielectric and the gyrotropic region is set to $h_d = 0.28\lambda_p$ and $h_g = 0.42\lambda_p$ yielding a total

height of $0.7\lambda_p$. The results obtained using Eq. (4) are shown in Fig. 7. The real part of

the propagation constant is independent of ε_d'' under the assumptions used in deriving
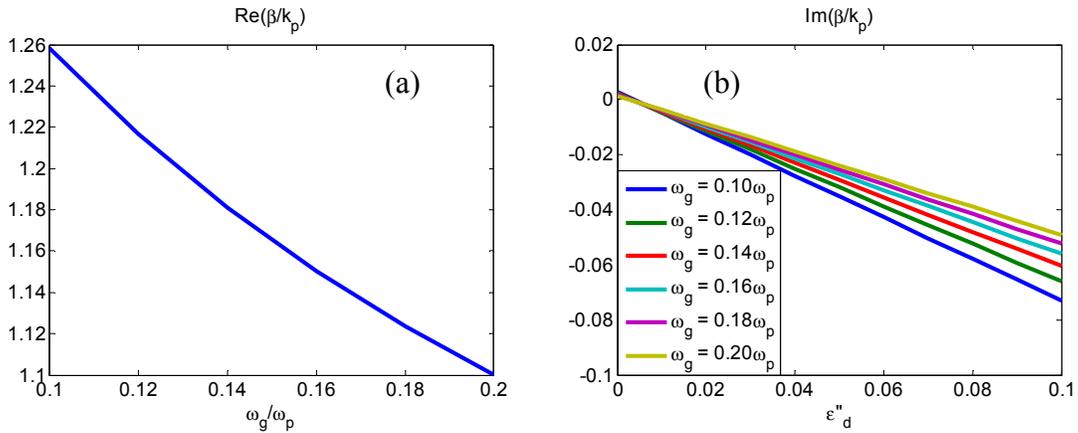

Figure. 7. (a) Real part of the propagation constant as a function of the magnetic bias (b) Imaginary part

of the propagation constant as a function of ε_d'' for various values of magnetic bias.

Eq. (4). As we can see in Fig. 6 the magnitude of β' decreases on increasing ω_g and this

decrease more than offsets the increase in magnitude of the first term in the expression

for β''. Consequently the magnitude of β'' decreases as we increase ω_g. This implies

that although increasing the magnetic bias makes it easier to compensate the intrinsic

losses in the plasmonic region further increase in ω_g results in a lower net gain since it

reduces the magnitude of both β' and β''.

C.   MODEL FOR SCATTERING PARAMETERS

Now that we have the equation for the propagation constant in the gyrotropic-dielectric waveguide we could use it to build a simplified model to evaluate the scattering parameter and effectively the amplifier gain for various setting of ε_d'' and ω_g. Consider an amplifier where the *transistor* region has a length of l and the propagation constant is β. The net amplifier gain can be expressed as follows.

$$G = |S_{11}|^2 = e^{-2\beta''l} e^{-C(\beta'')} \tag{5}$$

Where, $C(\beta'')$ represents the coupling losses at the interface between the transistor region and the waveguide region. As mentioned in the manuscript, one could argue that the loss in the plasmonic region is only one of the ways the incident signal could lose power and part of the incident signal could also be lost due to reflection. But with a properly designed AR layer we could ensure that none of the signal is reflected back and the only loss mechanism is through the absorption in the plasmonic region. At the interface between the input waveguide and the gyrotropic waveguide the interactions between the two waveguides result in the excitation of several higher-order evanescent modes in addition to the propagating modes. These modes also experience the losses in the plasmonic region and these losses are not accounted by β''. But these additional losses could be numerically evaluated and added to the model as a *coupling loss*, which is represented by the $C(\beta'')$. Furthermore we could make a series expansion in order to approximate $C(\beta'')$ and retain only the linear term.

$$C(\beta'') = -C_1\beta'' + C_0$$

This approximation is valid when the coupling losses depend weakly upon the both ε_d'' and ω_g and this is a valid approximation in the one-way regime. We could further make the substitution $C_1 = 2l_0$ and rewrite Eq. (5) in the following form.

$$\ln(G) = \ln|S_{11}|^2 = -2\beta''(l-l_0) - C_0 \tag{6}$$

Here, $l-l_0$ could be interpreted as an *effective length* that is shorter than the physical length due to the coupling losses at the interface. The two parameters, l_0 and C_0 can be obtained by fitting the equation to simulation data. Figure 8 shows the simulation results for the amplifier gain (G) for a range of gain coefficients, ε_d'', as a function of the transistor length (l).
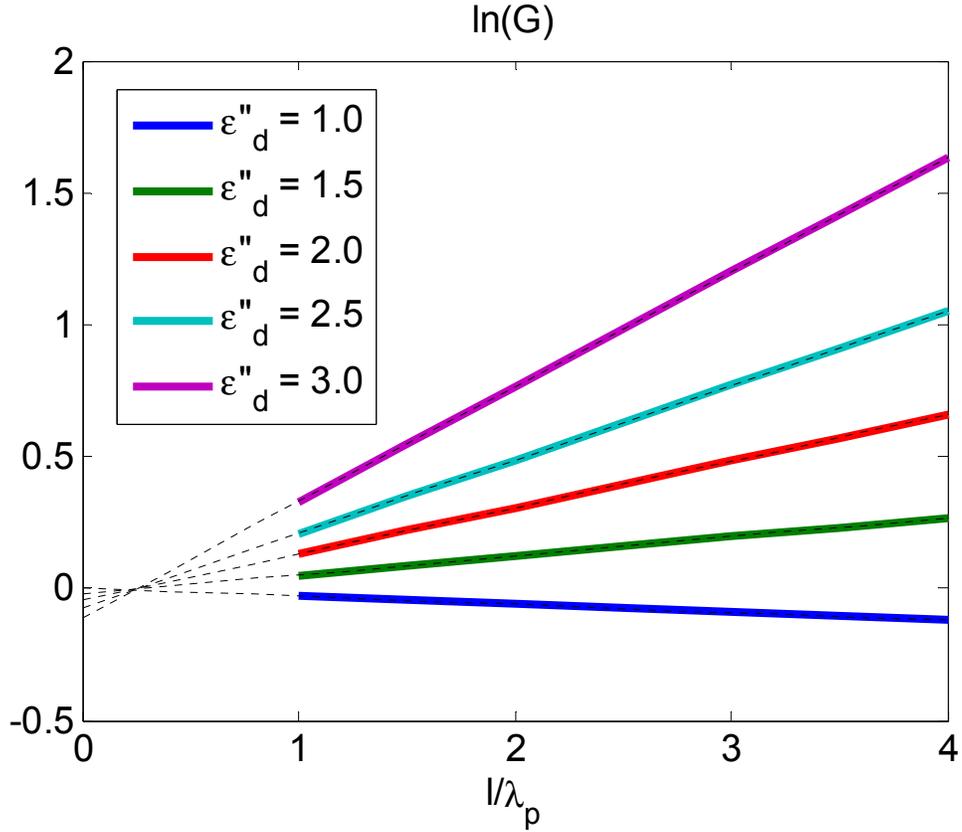
Figure. 8. Simulation results for the gain of the amplifier for various transistor lengths (l/λ_p) and gain coefficients (ε_d'').

The simulations were performed using a commercial full-wave FEM solver (COMSOL Multiphysics™). The details of the simulations are mentioned in the main manuscript. The simulation data shows excellent agreement with the linear regression fit. Interestingly all the linear fit lines converge at the same point justifying the use of Eq. (6) in fitting the data. The x-coordinate of the convergence point corresponds to l_0 while the y-coordinate corresponds to C_0. The fitting procedure provides the following results for the two fit parameters.

$$
\begin{aligned}
l_0 &= 0.238\lambda_p \\
C_0 &= 0.0044
\end{aligned}
\tag{7}
$$

In order to verify the effectiveness of the model we compare simulated amplifier gain values to the calculated one using the model given in Eq. (6) and using the parameters in Eq. (7). The propagation constant for the model was calculated with full dispersion given in Eq. (2) using the simplex method. The result of the comparison is shown in Fig. 9 and the full-wave simulation has an excellent agreement with the calculations using the model.

equation
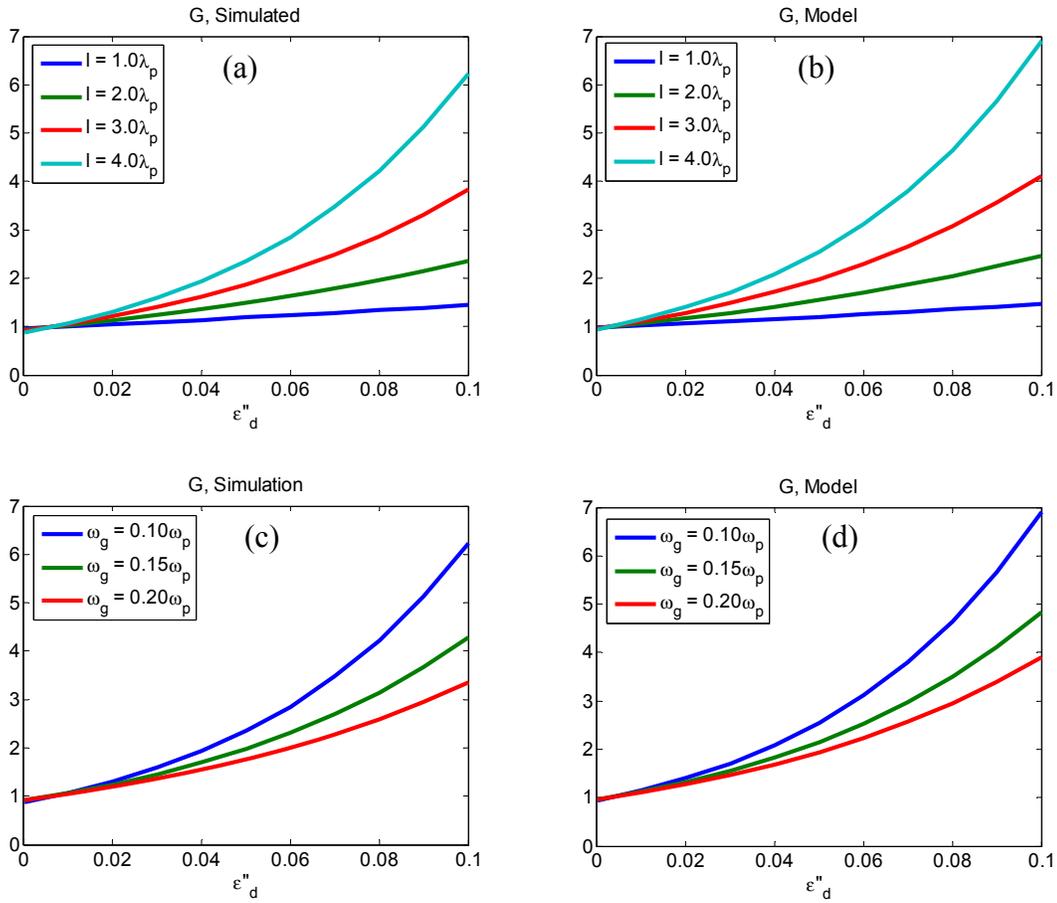
Figure. 9. Comparison of simulated gain (a,c) of the amplifier and gain calculated using the model (b,d) for various transistor lengths (l/λ_p) (a,b) and magnetic bias (ω_g/ω_p) (c,d). The amplifier gain is plotted against the gain coefficients (ε''_d) in all the plots.

References

1. Cai, W. & Shalaev, V. M. *Optical Metamaterials: Fundamentals and Applications*. (Springer, 2009).

2. Engheta, N. & Ziolkowski, R. W. *Metamaterials: Physics and Engineering Explorations*. (IEEE-Wiley, 2006).

3. Eleftheriades, G. V. & Balmain, K. G. *Negative-Refraction Metamaterials: Fundamental Properties and Applications*. (IEEE-Wiley, 2005).

4. Engheta, N. Circuits with light at nanoscales: optical nanocircuits inspired by metamaterials. *Science,* **317,** 1698–1702 (2007).

5. Engheta, N., Salandrino, A. & Alu, A. Circuit elements at optical frequencies: Nanoinductors, nanocapacitors, and nanoresistors. *Phys. Rev. Lett.* **95,** - (2005).

6. Engheta, N. Taming light at the nanoscale. *Phys. World* **23,** 31–34 (2010).

7. Engheta, N. From RF circuits to optical nanocircuits. *IEEE Microw. Mag.* **13,** 100–113 (2012).

8. Sun, Y., Edwards, B., Alù, A. & Engheta, N. Experimental realization of optical lumped nanocircuits at infrared wavelengths. *Nat. Mater.* **11,** 208–12 (2012).

9. Caglayan, H., Hong, S.-H., Edwards, B., Kagan, C. R. & Engheta, N. Near-Infrared Metatronic Nanocircuits by Design. *Phys. Rev. Lett.* **111,** 073904 (2013).

10. Alù, A., Young, M. & Engheta, N. Design of nanofilters for optical nanocircuits. *Phys. Rev. B* **77,** 144107 (2008).

11. Alù, A. & Engheta, N. All Optical Metamaterial Circuit Board at the Nanoscale. *Phys. Rev. Lett.* **103,** 143902 (2009).

12. Edwards, B. & Engheta, N. Experimental Verification of Displacement-Current Conduits in Metamaterials-Inspired Optical Circuitry. *Phys. Rev. Lett.* **108,** 193902 (2012).

13. Chettiar, U. K. & Engheta, N. Optical frequency mixing through nanoantenna enhanced difference frequency generation: Metatronic mixer. *Phys. Rev. B* **86,** 075405 (2012).

14. Alù, A. & Engheta, N. Input Impedance, Nanocircuit Loading, and Radiation Tuning of Optical Nanoantennas. *Phys. Rev. Lett.* **101,** 043901 (2008).

15. Luukkonen, O., Chettiar, U. K. & Engheta, N. One-Way Waveguides Connected to One-Way Loads. *IEEE Ant. Wirel. Propag. Lett.* **11,** 1398–1401 (2012).

16. Pozar, D. M. *Microwave Engineering*. (John Wiley, 2005).

17. Sedra, A. S. & Smith, K. C. *Microelectronic Circuits*. (Oxford university press, 1998).

18. Chen, W. *et al.* All-Optical Switch and Transistor Gated by One Stored Photon. *Science,* **341**, pp. 768-770 (2013).

19.   Miller, D. A. B. Are optical transistors the logical next step? *Nat. Photon.* **4,** 3–5 (2010).

20.   Noginov, M. A. *et al.* Compensation of loss in propagating surface plasmon polariton by gain in adjacent dielectric medium. *Opt. Express* **16,** 1385–92 (2008).

21.   Yu, Z., Veronis, G., Wang, Z. & Fan, S. One-Way Electromagnetic Waveguide Formed at the Interface between a Plasmonic Metal under a Static Magnetic Field and a Photonic Crystal. *Phys. Rev. Lett.* **100,** 023902 (2008).

22.   Maier, S. A. *Plasmonics: fundamentals and applications.* (Springer, 2007).

23.   Nezhad, M., Tetz, K. & Fainman, Y. Gain assisted propagation of surface plasmon polaritons on planar metallic waveguides. *Opt. Express* **12,** 4072–4079 (2004).

24.   Chettiar, U. K. & Engheta, N. Pulse compression in gyrotropic waveguides. *"In Prep.*

25.   Naik, G. V, Kim, J. & Boltasseva, A. Oxides and nitrides as alternative plasmonic materials in the optical range. *Opt. Mater. Express* **1,** 1090–1099 (2011).

26.   Yu, Z., Wang, Z. & Fan, S. One-way total reflection with one-dimensional magneto-optical photonic crystals. *Appl. Phys. Lett.* **90,** 121133 (2007).

27.   Ek, S., Lunnemann, P., Chen, Y., Semenova, E., Yvind, K. & Mork, J., Slow-light-enhanced gain in active photonic crystal waveguides. *Nature Communications,* 5:5039 (Sept 2014).

28. Grgicˊ, J., Raunkjær Ott, J., Wang, F., Sigmund, O., Jauho, A.-P., Mørk, J. & Mortensen, N. A. Foundamental limitations to gain enhancement in periodic media and waveguides, *Phys. Rev. Lett.* 108, 183903 (2012).